# Stability and deactivation of unconditioned Au/TiO$_2$ catalysts during CO oxidation in a near-stoichiometric and O$_2$-rich reaction atmosphere

Y. Denkwitz [a], Z. Zhao [a], U. Hörmann [b], U. Kaiser [b], V. Plzak [c], R.J. Behm [a,*]

[a] *Institute of Surface Chemistry and Catalysis, Ulm University, D-89069 Ulm, Germany*
[b] *Central Facility of Electron Microscopy, Ulm University, D-89069 Ulm, Germany*
[c] *Centre of Solar Energy and Hydrogen Research, Helmholtz Str. 8, D-89081 Ulm, Germany*

## Abstract

The deactivation of unconditioned Au/TiO$_2$ catalysts during CO oxidation at different reaction temperatures (30 and 80 °C) and in different reaction atmospheres was investigated. Kinetic and in situ IR spectroscopic measurements revealed a close correlation between the exponentially decreasing CO$_2$ formation rate and the CO$_{ad}$ coverage (decreasing) and carbonate coverage (increasing) during deactivation, whereas transmission electronic microscopy imaging revealed no significant changes in Au particle size. Consequences for the deactivation mechanism are discussed.
© 2007 Elsevier Inc. All rights reserved.

*Keywords:* CO oxidation; Conditioning; Deactivation; Gold catalysis

## 1. Introduction

Oxide-supported Au/MeO$_x$ catalysts, particularly Au/TiO$_2$ catalysts, have been shown to be highly active for various oxidation and reduction reactions already at low temperatures [1–3], the most prominent being the CO oxidation reaction [1,4–8]. But the technical application of these catalysts has been hindered by their rather low stability, that is, by their tendency for deactivation [9–11]. Recently, it was proposed that the activity of supported Au catalysts may be related to very small Au particles (see, e.g. [12]). Au/TiO$_2$ catalysts with very small Au particles, which turned out to be highly active for CO oxidation, were obtained by, for example, using the standard deposition–precipitation procedure described by Haruta [13], with subsequent drying in air at temperatures around 50 °C [14], rather than the more rigorous activation procedures commonly applied [8,15–18]. Interestingly, these unconditioned catalysts showed no measurable deactivation over reaction times of 50 h [14]. The high activity of these catalysts was attributed to the small size of the Au particles [14] rather than to cationic Au$^{\delta+}$ species that had been previously proposed as active species [6,19–23].

For comparison, highly active Au/TiO$_2$ catalysts pretreated by calcination at 400 °C in a 10% O$_2$/N$_2$ mixture (Au particle size about 2.5–3 nm) were found to deactivate rapidly during reaction at 80 °C [24]. The deactivation was attributed mainly to increased surface blocking due to carbonate formation, whereas the Au particle sizes were found to be rather stable [24]. The situation may be rather different for the much smaller Au particles on the unconditioned catalysts, which are expected to be much less stable, and particle growth may play a significant role. It may be speculated that particle growth results in activation rather than deactivation of the catalyst, following earlier proposals of an optimum Au particle size of about 3 nm [25]. In addition to structural effects induced by the CO oxidation reaction, changes in the surface chemical composition also may be important for the deactivation and may be responsible for the differences between unconditioned and calcined catalysts. So far, a direct comparison of the data on conditioned and unconditioned Au/TiO$_2$ catalysts has not been possible because of the different catalyst preparation procedures applied in these previous studies.

* Corresponding author.
  *E-mail address:* juergen.behm@uni-ulm.de (R.J. Behm).

To better understand the effects induced by catalyst conditioning on catalyst activity and stability and possibly also on the reaction mechanism, we investigated the deactivation behavior of an unconditioned $Au/TiO_2$ catalyst prepared in the same way as the conditioned $Au/TiO_2$ catalysts investigated previously [9,24], in a comparative study under different reaction conditions [26]. Besides following the activity for CO oxidation during time on stream at two different reaction temperatures (30 and 80 °C) and in two different reaction atmospheres (standard reaction atmosphere: $p_{CO}:p_{O_2} = 1:1$ and $O_2$-rich atmosphere: $p_{CO}:p_{O_2} = 1:20$)—that is, under conditions used in previous catalytic evaluation of unconditioned $Au/TiO_2$ catalysts [14]—we monitored the amount of adsorbed species by in situ diffuse reflectance infrared Fourier-transform spectroscopy (DRIFTS) in separate experiments performed under similar conditions. We evaluated possible reaction-induced changes in Au particle size by transmission electron microscopy (TEM) and X-ray photoelectron spectroscopy (XPS).

## 2. Experimental

### 2.1. Catalyst preparation

The catalyst was prepared by a deposition–precipitation procedure described previously [24,27]. In short, a commercially available $TiO_2$ powder (Degussa, P25) was suspended in water at 60 °C at a pH of 5–5.5. To this suspension, tetrachloroauric acid ($HAuCl_4 \cdot 4H_2O$) was added under vigorous stirring, with the pH kept constant by adding $Na_2CO_3$ solution. After an additional 30 min of stirring, the precipitate was cooled to room temperature, filtered, and washed. The precipitate was dried overnight at room temperature under vacuum and then for 8 h at 50 °C in air. The Au metal loading (3.1 wt% Au) was determined by inductively coupled plasma atom emission spectroscopy (ICP-AES). Before the experiments, the samples were heated to reaction temperature (30 or 80 °C) in a $N_2$ stream and kept at that temperature for 30 min.

### 2.2. Catalyst characterization

The sizes and distribution of the Au particles were determined by TEM using a Philips CM 20 microscope (operating at 200 kV). Typically, 500 to >1000 particles were evaluated for each sample. The relative concentrations and the oxidation states of Au, Ti, and O were determined by X-ray photoelectron spectroscopy (XPS; PHI 5800 ESCA system), using monochromatized Al$K_\alpha$ radiation. Spectra of the catalyst were recorded before reaction in the nonconditioned state and after 2000 min of CO oxidation under various conditions. The binding energies (BEs) were calibrated with respect to that of bulk Ti(2p$_{3/2}$) (459.2 eV for Ti$^{4+}$ [28]). Shirley background subtraction and peak fitting were performed using a public XPS peak fit program (XPSPEAK4.1; R Kwok). For fitting the Ti(2p) peak, the difference between Ti(2p$_{3/2}$) and Ti(2p$_{1/2}$) was set to 5.71 eV, and the integral intensity of the Ti(2p$_{1/2}$) was assumed to be half of the Ti(2p$_{3/2}$) intensity. For the Au(4f) peak, the difference between Au(4f$_{7/2}$) and Au(4f$_{3/2}$) was set to 3.67 eV, and the integral intensity of the Au(4f$_{5/2}$) was 3/4 that of the Au(4f$_{7/2}$) peak.

### 2.3. Activity measurements

Activity measurements were carried out at atmospheric pressure in a quartz tube microreactor under differential reaction conditions, with typically 65–70 mg of diluted catalyst powder. To limit the conversion to values typically between 5 and 20%, the catalyst was diluted with $\alpha$-$Al_2O_3$, which is not active for CO oxidation. The experiments were carried out with a gas flow of 60 Nml min$^{-1}$ at 30 and 80 °C, respectively, in the different gas mixtures. The gas mixtures were prepared by mass flow controllers (Hastings HFC-202). Incoming and effluent gases were analyzed by online gas chromatography (Dani GC 86.10HT or CHROMPACK CP9001), using $H_2$ as the carrier gas. High-purity reaction gases (CO 4.7, $O_2$ 5.0, and $N_2$ 6.0; Westphalen) were used. The reaction rates were determined based on the $CO_2$ partial pressure; for more information on the measurements, see [29]. Mass and heat transport effects were negligible, because the rates were <10$^{-5}$ mol s$^{-1}$ cm$^{-3}$; for details, see [30].

### 2.4. Infrared measurements

In situ IR measurements were performed by DRIFTS using a commercial in situ reaction cell unit (Harricks HV-DR2) [31]. The spectra were recorded in a Magna 560 spectrometer (Nicolet) equipped with a MCT narrow-band detector. Gas mixtures were prepared in a similar way as described above, using 14–24 mg of $\alpha$-$Al_2O_3$ diluted catalyst (dilution 1:5) as a catalyst bed. Typically, 400 scans (acquisition time, 3 min) were co-added for each spectrum. The intensities were evaluated in Kubelka-Munk units (KMU), which are derived from the reflectance $R_\nu$ via KMU$_\nu = (1 - R_\nu)^2/2R_\nu$ and are linearly related to the adsorbate concentration for a wide range of experimental conditions [32,33]. A detailed discussion of possible deviations from this linear relation has been given previously [33]. Background subtraction and normalization of the spectra were performed by subtracting spectra recorded in a flow of $N_2$ at the reaction temperature just before starting CO oxidation. To remove changes in the reflectivity, the spectra were scaled to a similar intensity at 2430 cm$^{-1}$, which did not interfere with any other signals, and where the shape of the raw spectrum changed little during the measurements. The gas-phase CO signal was removed by subtracting a spectrum obtained on pure $\alpha$-$Al_2O_3$ in CO-containing atmosphere. For simultaneous analysis of the gas flow, a gas chromatograph (CHROMPACK CP9001) was connected to the exhaust of the DRIFTS cell.

## 3. Results

Fig. 1 illustrates the deactivation of the unconditioned catalyst during reaction under different reaction conditions in both a standard reaction mixture (1% CO, 1% $O_2$, balance $N_2$) and
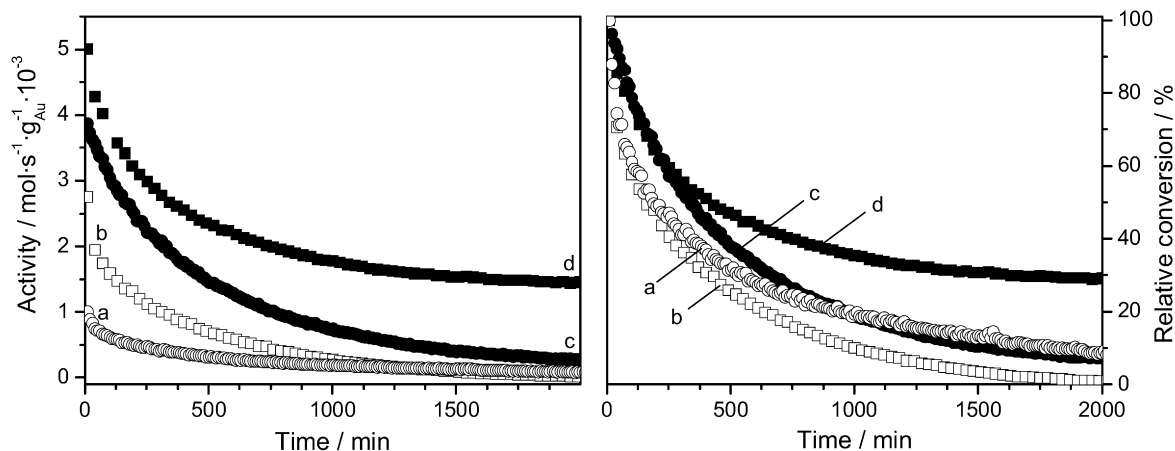
Fig. 1. Evolution of the mass-specific CO oxidation rate (left panel) and the relative conversion (right panel) on an unconditioned Au/TiO$_2$ catalyst during 2000 min reaction at 30 °C (a, b) and 80 °C (c, d) in standard reaction mixture (a, c) and in O$_2$-rich atmosphere (b, d).

Table 1
Absolute and relative activity, mean particle size, Au(4f):Ti(2p) intensity ratio as well as CO$_{ad}$, CO$_2$ and carbonate related IR intensities of the unconditioned Au/TiO$_2$ catalysts and after 2000 min reaction under different reaction conditions

| Catalyst | Initial/final activity ($10^{-3}$ mol g$_{Au}$) | Activity after 1000/2000 min reaction (%) | Mean Au particle size (nm) | Au(4f):Ti(2p) ratio | Initial/final CO$_{ad}$ related IR intensity (KMU) | Initial/final CO$_2$ related IR intensity (KMU) | Initial/final carbonate related IR intensity (KMU) |
|---|---|---|---|---|---|---|---|
| Dried catalyst | – | – | $1.3 \pm 0.4$ | $0.21 \pm 0.02$ | – | – | – |
| After 2000 min reaction at 30 °C, 1% O$_2$ | 1.0/0.09 | 19/9 | $1.9 \pm 0.9$ | $0.21 \pm 0.02$ | 4.29/0.40 | 0.79/0.06 | 7.3/44.5 |
| After 2000 min reaction at 80 °C, 1% O$_2$ | 3.9/0.3 | 20/7 | $1.8 \pm 0.7$ | $0.18 \pm 0.02$ | 1.22/0.35 | 1.76/0.92 | 5.7/45.4 |
| After 2000 min reaction at 30 °C, 20% O$_2$ | 2.8/0.03 | 10/1 | $2.0 \pm 1.0$ | $0.20 \pm 0.02$ | 2.61/0.06 | 1.08/0.01 | 5.9/35.9 |
| After 2000 min reaction at 80 °C, 20% O$_2$ | 5.0/1.5 | 35/29 | $1.8 \pm 0.7$ | $0.18 \pm 0.02$ | 0.36/0.06 | 2.37/1.36 | 5.0/41.7 |

an O$_2$-rich atmosphere (1% CO, 20% O$_2$, balance N$_2$) and at both 30 and 80 °C. The left panel depicts the evolution of the activity under these reaction conditions, described by the mass specific rate under differential reaction conditions, with time on stream. The absolute value of the (initial) activity at 80 °C agrees quantitatively with that reported by Willneff et al. on similarly prepared catalysts under comparable reaction conditions [14]. The right panel shows the deactivation on a relative scale, relative to an initial activity of 100%. In all cases, the activity decreased in an approximately exponential way to a near–steady-state value. Both the initial activity and the steady-state activity were higher at 80 than at 30 °C; the ca. threefold increase in the steady-state activity in the standard reaction mixture (50-fold in the O$_2$-rich gas mixture) corresponds to formal activation energies of 20 and 72 kJ mol$^{-1}$, respectively. For the initial activities, the corresponding values were 24 and 11 kJ mol$^{-1}$ (fourfold and twofold increases) (see Table 1). The relative decay was higher at the reaction temperature of 30 than at 80 °C, lower in the O$_2$-rich atmosphere than in the standard reaction atmosphere at 80 °C, but higher in the

O$_2$-rich atmosphere than in the standard reaction atmosphere at 30 °C. These findings would agree with an explanation attributing the lower deactivation in an O$_2$-rich atmosphere to enhanced decomposition of surface-blocking carbonate species, whereas at 30 °C, this reaction in not yet active. This tentative proposal was evaluated by DRIFTS observations as described below.

TEM measurements performed before and after the reaction revealed a homogeneous distribution of very small Au nanoparticles (Fig. 2a) with a wide particle size distribution, ranging from subnanometer up to ca. 8 nm. After drying in air, before any subsequent reaction, the particle size distribution (Fig. 2b) resulted in a mean particle size of $1.3 \pm 0.4$ nm. During the CO oxidation reaction, the mean particle size increased slightly, by about 0.5 nm over 2000 min (see Figs. 2c–2f). The increase was correlated with a further widening of the particle size distribution; however, the reaction conditions (e.g., reaction atmosphere, reaction temperature) had little effect. Intuitively, we might have expected to find more pronounced particle growth, at least for reaction in the O$_2$-rich atmosphere, considering the
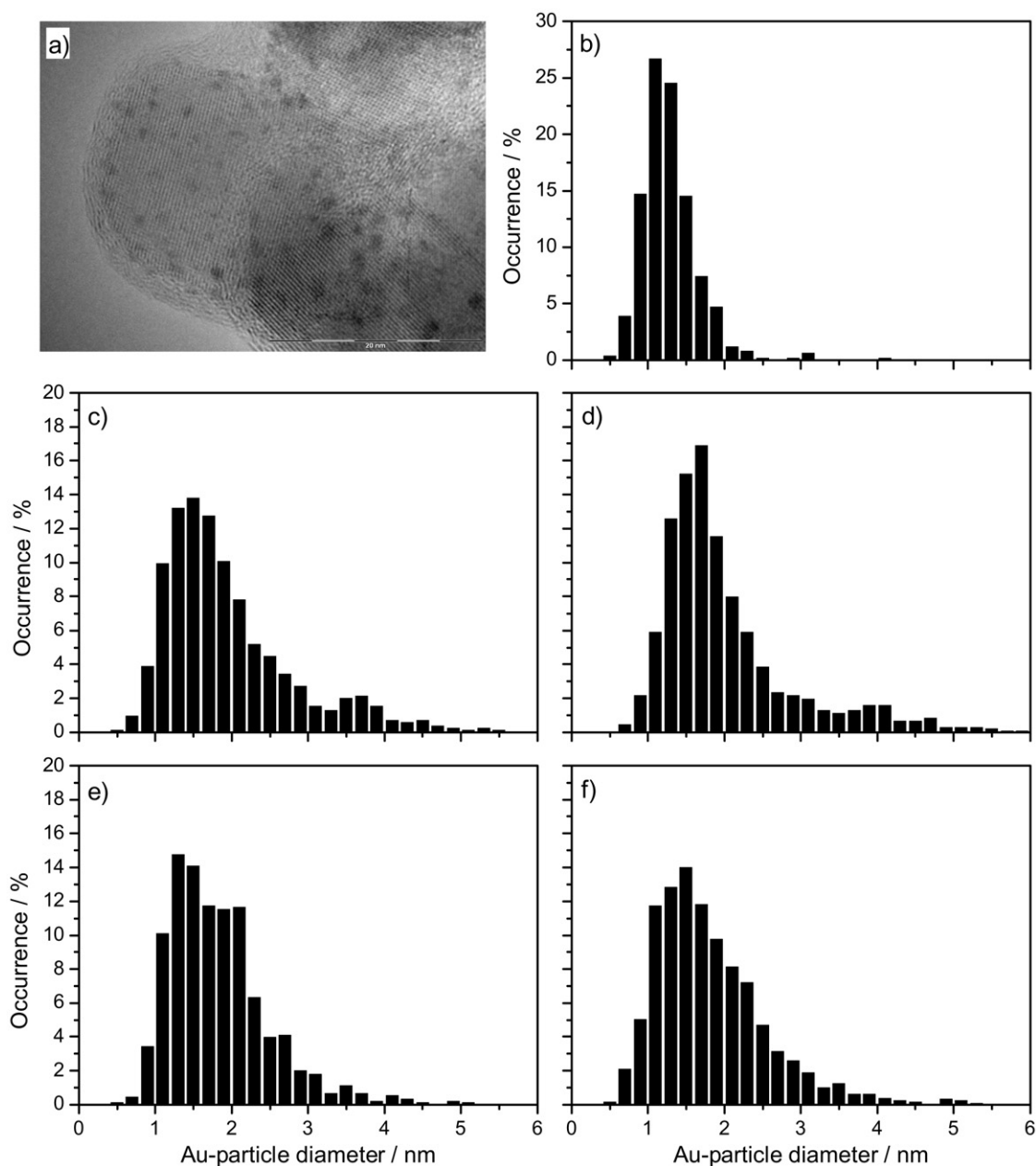
Fig. 2. TEM image (a) and particle size distribution (b–f) of the unconditioned Au/TiO$_2$ catalyst before reaction (a, b), and after 2000 min reaction at 30 °C (c, d) and 80 °C (e, f) in standard reaction mixture (c, e) and O$_2$-rich atmosphere (d, f).

enhanced particle growth on calcination in O$_2$, both for realistic Au/TiO$_2$ catalysts [24] and for Au/TiO$_2$(110) model catalysts [34]. But apparently, the much lower reaction temperature (80 °C, compared with the calcination temperature of 400 °C) was too low for more pronounced particle growth. This agrees well with previous observations of a much lesser Au particle growth on calcination at 200 [18] or 300 °C [24]. The present results demonstrating very little Au particle growth during reaction at 80 °C should not be confused with previous observations of negligible Au particle growth at 80 [24] and also at 180 °C [35] on catalysts that were calcined before reaction. In the latter case, pretreatment led to much more stable Au particles with particle sizes of ∼3 nm, compared with ∼1.3 nm in the present unconditioned catalysts.

Reaction induced changes in the surface composition of the supported catalyst were characterized by XPS (see Fig. 3 and Table 1). Survey spectra (Fig. S1 in Supplementary material) recorded after drying in air and after the different reaction treatments show peaks related to Ti, O, and Au as well as some C(1s) intensity at BEs compatible with carbon surface contamination picked up during transport through air (285 eV) and surface carbonates (289 eV). Detailed spectra recorded in the Ti(2p) and Au(4f) regions revealed the following trends. The Ti(2p) spectra showed completely oxidized Ti$^{4+}$ species (459.2 eV [28]; Fig. 3, left panel) before and after reaction, indicating that within the sensitivity range of the measurement, while drying in air the support was already fully oxidized, and that this state did not change during subsequent reaction in the CO:O$_2$ mixtures
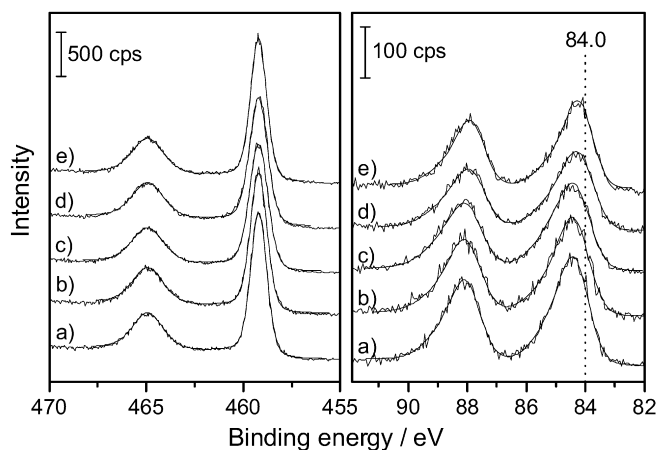
Fig. 3. XP spectra of the unconditioned $Au/TiO_2$ catalyst, before reaction (a), and after 2000 min reaction at 30 °C (b, c) and 80 °C (d, e) in standard reaction mixture (b, d) and $O_2$-rich atmosphere (c, e). The left and right panels show the Ti(2p) and Au(4f) regions, respectively.

used. In the Au(4f) region (Fig. 3, right panel), all samples exhibited a broad (FWHM ~1.5 eV), slightly asymmetric signal with maximum $Au(4f_{7/2})$ peaks at about 84.4 eV for the catalyst before reaction and 84.4/84.3 eV after reaction at 30 and 80 °C, respectively. The peak shift and the broadening of the Au(4f) peak can originate from coexistent cationic and metallic Au species (initial state effect) [12,36] and/or the very small size of the metallic Au particles (final state effect) [37]. In a recent in situ XPS study on a unconditioned catalyst, which equally yielded broad, up-shifted Au(4f) peaks, the authors explained the peak structure by one state at 84.3 eV and an additional, broader component centered at 85.2 eV, indicative of two Au species that they described as nonionic [14]. Considering that, based on the TEM results, the catalyst contained very small Au particles with a continuous and a rather wide particle size distribution of around 1.3–2.0 nm, and that recent XPS measurements found clear peak shifts for Au particles of sizes comparable to the present ones [38], final state shifts must be expected for our Au(4f) data. Furthermore, these shifts differ for different particle sizes, which, due to integration over these different contributions, leads to a wide peak as was observed experimentally. Whereas these final state effects would be sufficient to explain the observed peak shift and peak broadening [38], a slight positive charge on the Au particles (due, e.g., to chemical interaction with the support) cannot be ruled out based on our data. However, a combination of a cationic $Au^{\delta+}$ state and of a fully metallic $Au^0$ state, requiring particles >3 nm in diameter, is not compatible with the TEM data and thus is excluded. This interpretation is supported by the DRIFTS results discussed below, which showed only C–O signals with frequencies characteristic of CO adsorbed on metallic $Au^0$ particles.

Further information on the distribution of the two components and the Au particle size can be obtained from the respective peak intensities or, equivalently, the Au(4f)/Ti(2p) intensity ratios. These are essentially identical before and after reaction (see Table 1), which also points to negligible changes in the distribution and size of the Au particles during reaction.

Finally, the accumulation of adsorbed surface species was followed by in situ DRIFTS measurements performed during the reaction. Fig. 4 illustrates the resulting signal intensities due to changes in surface composition in the sets of DRIFT spectra recorded during the reaction in the standard reaction mixture at 30 and 80 °C. The spectra reveal characteristic peaks at 2112–2120 $cm^{-1}$ (CO adsorbed on metallic Au), at 2339 and 2361 $cm^{-1}$ (gaseous $CO_2$), and a set of vibrational features in the range of 1200–1550 $cm^{-1}$, where the latter are commonly assigned to the C=O stretch vibration $\nu$(C=O) of bidentate carbonates (~1527 $cm^{-1}$), the symmetric stretch vibration $\nu_s$(COO) of monodentate carbonates (1359 $cm^{-1}$), and the asymmetric stretch vibration $\nu_{as}$(COO) of monodentate carbonates (1430–1530 $cm^{-1}$), which is hidden under the C=O stretch vibration of bidentate carbonates. The same holds true for the asymmetric stretch vibration of carboxylates (for which the peak should appear at 1560–1620 $cm^{-1}$), whereas the symmetric stretch vibration appears at 1406 $cm^{-1}$ [39–41]. With increasing reaction time, the $CO_{ad}$- and $CO_2$-related peaks decreased in intensity, whereas the carbonate related signals increased significantly. The small peak at 2170 $cm^{-1}$ (Fig. 4, top left), due to gas-phase CO absorption, was not considered in the subsequent intensity determination. The general shapes of the $CO_{ad}$- and $CO_2$-related peaks did not change with time, indicating that the nature of the adsorbed CO species and thus of the adsorption sites was not modified by the reaction. However, the peak frequency of the C–O vibration shifted to slightly higher frequencies from 2112 to 2114 $cm^{-1}$ with reaction time, simultaneous with the pronounced loss in intensity, pointing to a decrease in the local density of the CO adlayer on the Au nanoparticles with time [42]. This situation was different for the broad peak in the wavenumber region 1200–1700 $cm^{-1}$. The intensity of the adsorbed carbonate and carboxylate species increased during the reaction. At the beginning of the reaction (after 15 min; see Fig. 4 top right), the intensities of the peaks at 1359, 1406, and 1527 $cm^{-1}$ were about equal. With increasing reaction time, the intensity of the peak at ~1527 $cm^{-1}$ increased strongly and became significantly more pronounced than those of the former two peaks. The stronger intensity increase of the peak at 1527 $cm^{-1}$ can be explained by the fact that this peak comprises contributions from all three species (monodentate and bidentate carbonates as well as carboxylates), whereas the other two peaks are specific for monodentate carbonate (1359 $cm^{-1}$) and carboxylate (1406 $cm^{-1}$). In principle, it should be possible to subtract the varying contributions from the latter two species to the 1527 $cm^{-1}$ peak by comparing them with the intensity variation of the other two peaks, but in practice this is not possible, because of the large overlap between these peaks (see Fig. 4). On a qualitative scale, the monodentate carbonate signal at 1359 $cm^{-1}$ was found to increase under all reaction conditions, whereas the carboxylates were less stable at 80 °C (less intensity increase with time compared with the monodentate carbonate signal), and the contribution of bidentate carbonates was difficult to evaluate.

Because the catalyst was not conditioned, both water and OH groups were present on the catalyst before reaction. This is indicated by, for example, the background spectrum, with sig-
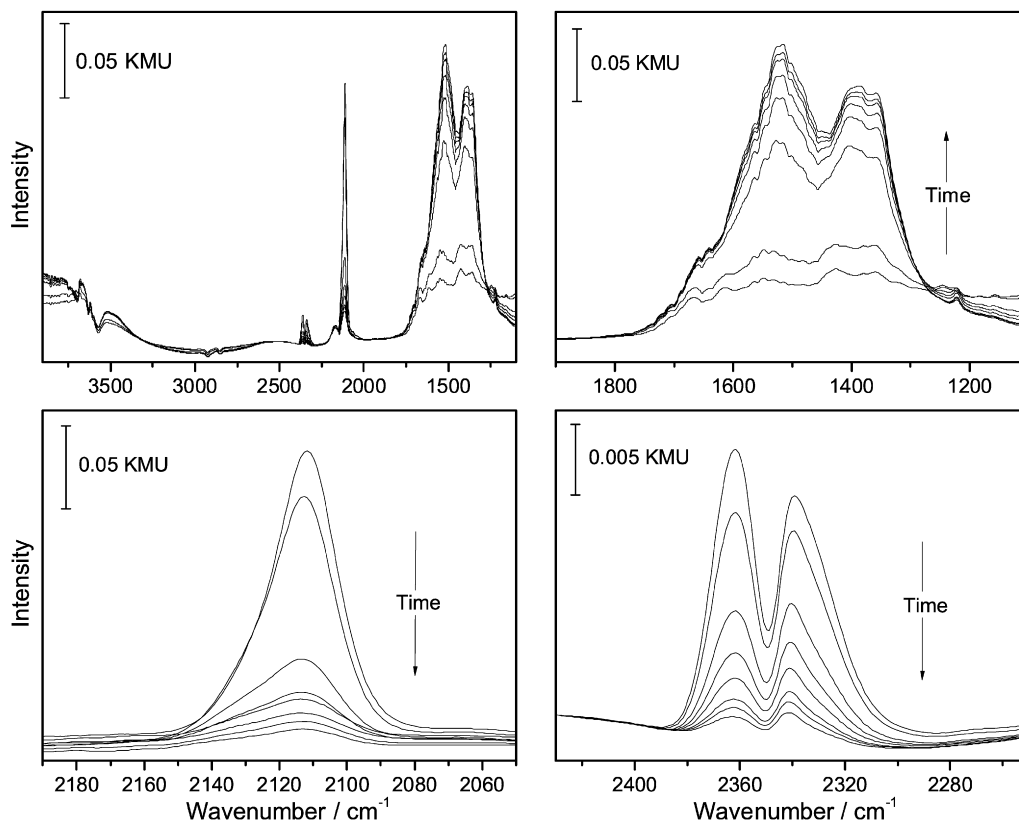
Fig. 4. Sequence of in situ DRIFT spectra recorded during CO oxidation on an unconditioned Au/TiO$_2$ catalyst in a standard reaction mixture at 30 °C (reaction times: 15, 70, 700, 970, 1330, 1600, and 2020 min). Top left: complete spectra, top right: enlarged detail of the O–C–O bending region ('carbonate region'), bottom left: enlarged detail of the C–O stretch region characteristic for CO$_{ad}$, bottom right: enlarged detail of the C–O stretch region characteristic for CO$_2$.

nals of isolated OH groups at 3724 and 3675 cm$^{-1}$ [43–45], of the HOH mode of adsorbed water at ~1630 cm$^{-1}$, and of the OH vibration at 2500–3300 cm$^{-1}$. These signals did not increase with reaction time (Supplementary material, Fig. S2, right panel); thus, an accumulation of H$_2$O from the gas feed can be excluded. In fact, the latter signals decrease slightly at the beginning of the reaction, indicative of a slight loss of H$_2$O at this time, and then remain of constant intensity. The initial consumption of water can be most easily explained by some limited formation of bicarbonate species, which would also agree with the observed peak at ~1250 cm$^{-1}$ ($\nu_\delta$(C–OH) of bicarbonate) [46]. The latter feature also could arise from the $\nu_{as}$(COO) vibration of bidentate carbonate, however [39]. Finally, the formate-related C–H vibration appearing at 2800–3000 cm$^{-1}$, remained essentially unchanged during the reaction, indicating that formate buildup did not occur under the present reaction conditions. Accordingly, these species also were not affected by the ongoing CO oxidation.

For reactions under different reaction conditions (spectra not shown), at 30 and at 80 °C in O$_2$-rich and standard atmospheres, the characteristic features were similar, with only the exact frequency values and the intensities and their evolution during reaction being somewhat different. This is evident in the CO$_{ad}$-related peak, which appears at 2112 cm$^{-1}$ for CO oxidation in the standard reaction mixture at 30 °C and varies between 2120 and 2112 cm$^{-1}$ for different reaction conditions. In all cases, the frequencies remained constant over time, while the intensity

decreased. Thus, under all reaction conditions, CO adsorption was observed only on metallic Au$^0$ particles during reaction. The intensity of the carboxylate species was less pronounced at 80 than at 30 °C.

The temporal evolution of the different peak intensities during reaction is illustrated in Figs. 5 and 6, where the integrated intensity of the CO$_{ad}$, CO$_2$, and carbonate-related peaks at 2112–2120, 2339–2361, and 1516–1527 and 1359 cm$^{-1}$, respectively, are plotted as functions of time. (For the carbonate, related intensity was determined by integrating the intensity between 1270 and 1750 cm$^{-1}$.) Fig. 5 shows the evolution of these intensities with reaction time for reaction in standard reaction mixture and in O$_2$-rich atmosphere at 30 °C. For the carbonate intensity, we also included the inverted development of the intensity with time (designated by crosses). We found an almost exponential decay of the CO$_{ad}$- and CO$_2$-related intensities and a similar increase in the carbonate-related intensity over time (see also the inverted carbonate intensity), independent of the reaction atmosphere (Fig. 5). As expected, the CO$_2$-related intensity was significantly higher in the O$_2$-rich atmosphere than in the standard atmosphere, whereas the CO$_{ad}$ intensity decreased to about half when going to the O$_2$-rich atmosphere. However, the final steady-state intensity after 2000 min was significantly lower for the CO$_{ad}$- and CO$_2$-related intensity in the O$_2$-rich atmosphere than in the standard reaction atmosphere, on both an absolute scale (Fig. 5, left panel) and a relative scale (Fig. 5, right panel). The increases in the carbonate intensity
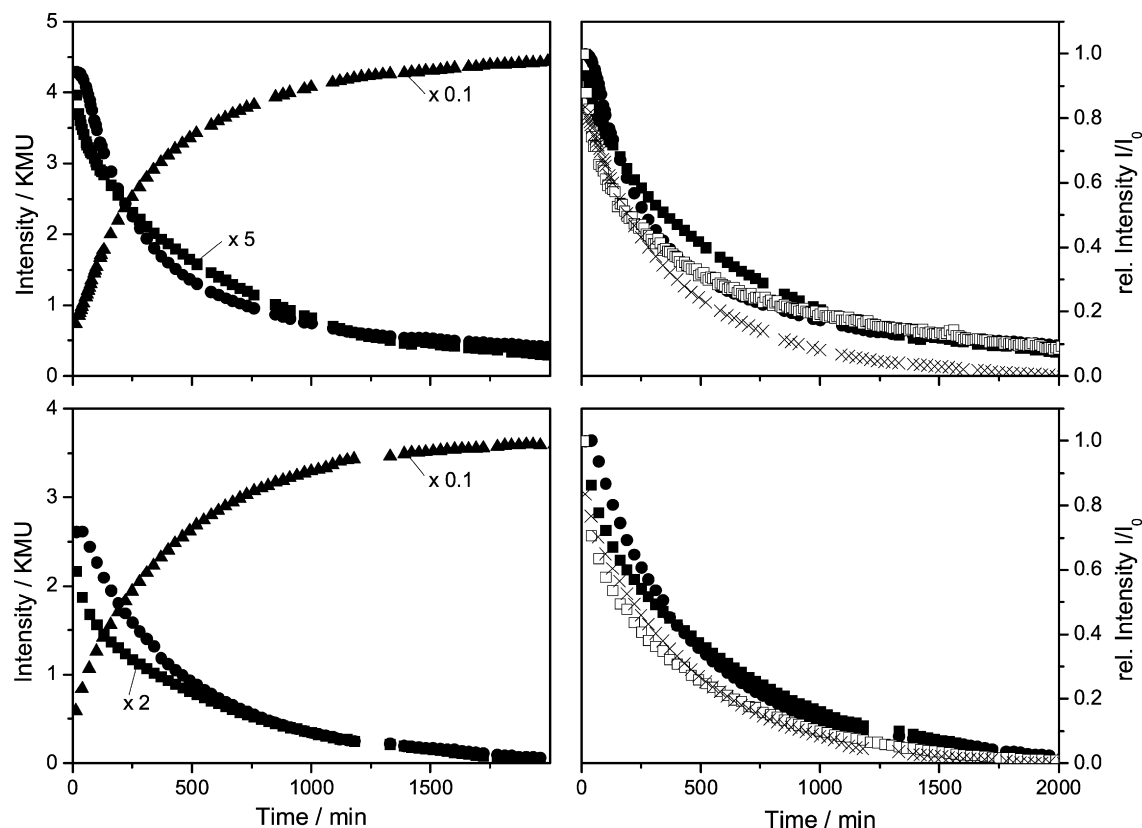
Fig. 5. Intensity of the DRIFTS signals characteristic for $CO_{ad}$ (●), $CO_2$ (■), and carbonate (▲) as function of time during CO oxidation on an unconditioned Au/$TiO_2$ catalyst at 30 °C in standard reaction atmosphere (left upper panel) and in $O_2$-rich atmosphere (left lower panel). The decay of the respective relative intensities, the inverted carbonate intensity (×) and, for comparison, of the $CO_2$ formation activity (□), is depicted in the right panels.

and hence in the net carbonate formation were about similar in both atmospheres (Fig. 5, left panel). In both atmospheres, the decay of the $CO_{ad}$-related signal with time closely resembled that of the $CO_2$ signal, and the relative activity measured under differential reaction conditions (data taken from Fig. 1) closely followed the relative activities of these signals (Fig. 5, right panel), indicative of a close correlation between $CO_{ad}$- and $CO_2$-related signals and the CO oxidation activity under otherwise similar conditions.

Fig. 6 plots the corresponding trends of the intensities for reaction at 80 °C. Again, the $CO_{ad}$- and $CO_2$-related intensities decayed continuously (Fig. 6, left panel), but compared with reaction at 30 °C, the agreement with an exponential decay was less good and the decay was less rapid (Fig. 6, right panel). Furthermore, the steady-state values were much higher. The much slower decay and the finite steady-state value of the $CO_{ad}$- and $CO_2$-related intensities agree well with the behavior of the differential activity, which also approached a finite steady-state value (Fig. 6).

The most pronounced differences between 30 and 80 °C were obtained for the evolution of the carbonate-related intensity. At the reaction temperature of 80 °C, it increased in an approximately linear way over the full course of the experiment in both the standard reaction mixture and the $O_2$-rich reaction atmosphere. The initial increase was less steep than at 30 °C, but the intensities reached after 2000 min were significantly greater than the saturation intensities obtained at 30 °C.

It should be noted that due to the higher catalyst activity at 80 °C, we could not perform the higher-temperature DRIFTS measurements under differential reaction conditions. The minimum amount of catalyst required to obtain sufficient IR intensity resulted in an initial conversion of ca. 72% for the standard reaction atmosphere and 94% for the $O_2$-rich atmosphere. Therefore, we also included the conversion measured by GC at the exit of the DRIFTS reaction cell in the plot (open circles in Fig. 6, right panel). In that case, the activity decreases (to 71% in standard reaction atmosphere and 88% in $O_2$-rich atmosphere) were much less pronounced than those under differential reaction conditions, and the decay was more linear. But because the IR signals were obtained from the top layer of the catalyst bed in the DRIFTS reaction cell, where the reaction conditions should correspond closely to the inlet gas composition and thus also to the gas composition under differential reaction conditions, the DRIFTS intensities should be more correlated with the activity behavior under differential reaction conditions, with some deviation toward the behavior measured at the exit of the DRIFTS reaction cell.

Finally, we followed the effect of raising the reaction temperature from 30 to 80 °C during the reaction after close to steady-state conditions were reached at the lower reaction temperature. The resulting changes in the IR intensities are illustrated in Fig. 7; note that the first 2000 min were identical to those shown in Fig. 5. In the standard reaction atmosphere, raising the temperature to 80 °C resulted in an instantaneous in-
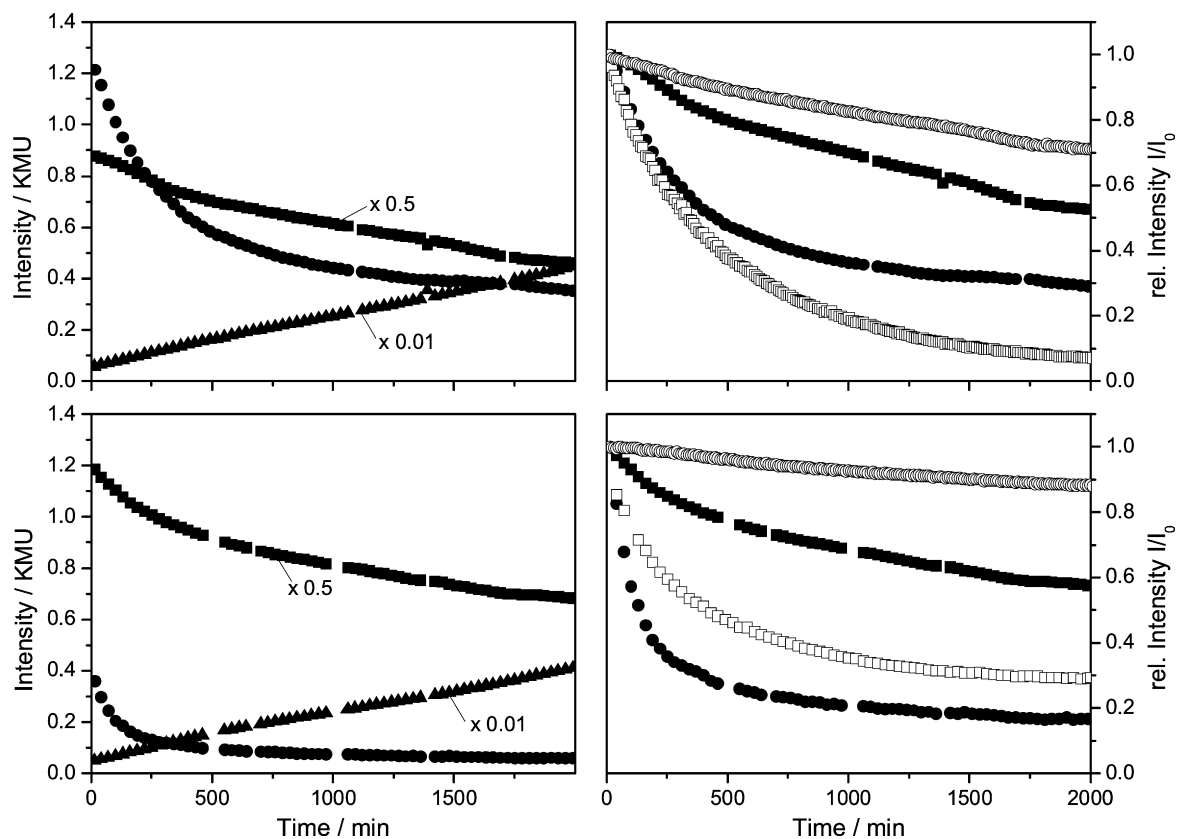
Fig. 6. Intensity of the DRIFTS signals characteristic for $CO_{ad}$ (●), $CO_2$ (■), and carbonates (▲) as a function of time during CO oxidation on an unconditioned Au/TiO$_2$ catalyst at 80 °C in standard reaction atmosphere (left upper panel) and in O$_2$-rich atmosphere (left lower panel). The decay of the respective relative intensities and, for comparison, of the activity measured under differential reaction conditions (□) and at the exit of the DRIFTS cell (○), respectively, is depicted in the right panels.
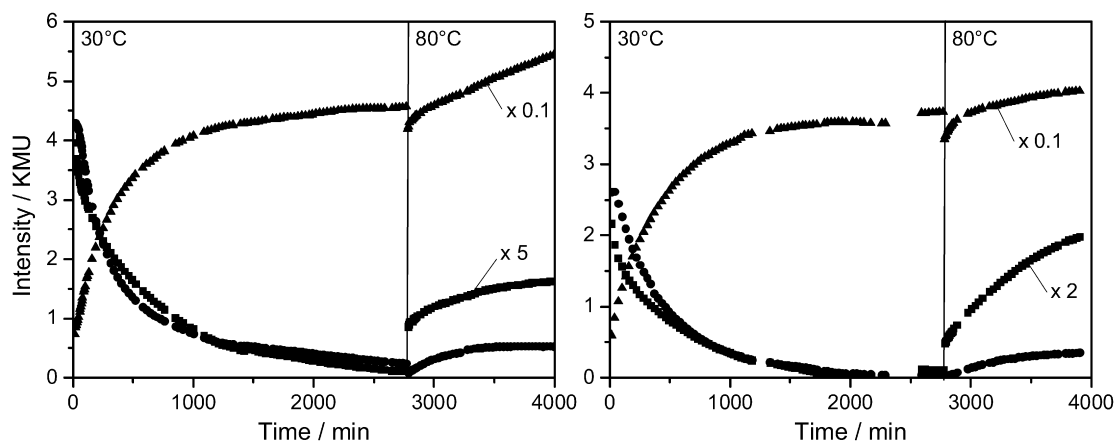


Fig. 7. Intensity of the DRIFTS signals characteristic for $CO_{ad}$ (●), $CO_2$ (■), and carbonates (▲) as function of time during CO oxidation on an unconditioned Au/TiO$_2$ catalyst at 30 °C and subsequent temperature increase to 80 °C in standard reaction atmosphere (left panel) and in O$_2$-rich atmosphere (right panel).

crease in the $CO_2$ intensity by about a factor of 7, followed by a slower intensity increase over time. In contrast, the $CO_{ad}$ intensity first dropped by 65% and then increased in a close to similar way as the $CO_{ad}$-related intensity. The carbonate intensity also dropped initially and then increased with time in an almost linear fashion. Thus, in all cases the intensity increased with time with increasing temperature. The distinct difference between $CO_{ad}$ intensity (decrease) and $CO_2$ intensity (pronounced in-

crease) directly after the temperature increase can be explained in a simple way: The $CO_2$ formation rate and hence the $CO_2$ concentration increased instantaneously due to thermal activation of the reaction. The $CO_{ad}$ coverage, on the other hand, decreased initially due to thermal desorption. The subsequent slow intensity increase in both the $CO_{ad}$ and the $CO_2$ signal over time until a saturation value was reached, together with the linear increase in carbonate intensity, indicates that after the

temperature change, the balance between carbonate adlayer and CO adlayer/CO oxidation activity was modified (see the discussion below).

For reaction in the $O_2$-rich atmosphere (Fig. 7, right panel), the effect of changing to 80 °C was qualitatively comparable, but the increase in $CO_2$ rate with time at 80 °C after the initial rise by about a factor of 5 reflecting the thermal activation, was much more pronounced than in the standard reaction atmosphere. The $CO_{ad}$ intensity first dropped by 54% and then also increased with time, but much more slowly than the $CO_2$-related intensity. Finally, for the carbonate-related intensity, the change in intensity with time was much less pronounced than for reaction in standard reaction atmosphere, pointing to a much lower steady-stare intensity (and coverage) of surface carbonates at 80 °C in $O_2$-rich reaction atmosphere than in standard reaction atmosphere, whereas for reaction at 30 °C, the steady-state intensities appeared rather similar. It should be noted that, as discussed in connection with Fig. 6, at 80 °C, differential reaction conditions were no longer adhered to, but nevertheless we would expect a gas composition at the upper layer close to that at the inlet. In total, these experiments demonstrated that in an $O_2$-rich atmosphere, the growth of carbonates at 80 °C was much less pronounced than in the standard reaction atmosphere, pointing to an enhanced $O_2$-induced carbonate decomposition, and that the simultaneous increase in $CO_{ad}$ and $CO_2$ intensity on the one hand and in carbonate intensity on the other hand after changing to 80 °C indicates an altered balance between carbonate adlayer and CO adlayer/CO oxidation activity compared with the situation at 30 °C. A different relationship between carbonate coverage and $CO_{ad}$ coverage/$CO_2$ formation rate at 30 and 80 °C also was obvious from the evolution of the related intensities with time at these temperatures (see Figs. 5 and 6). Thus, after the temperature was changed to 80 °C, the system approached a new steady-state situation that was at least qualitatively comparable to that reached after a sufficiently long reaction at 80 °C directly.

## 4. Discussion

The data presented above lead us to draw the following conclusions regarding the reaction and deactivation behavior of unconditioned P25-based Au/TiO$_2$ catalysts in the CO oxidation reaction:

1. The absolute activity of the unconditioned catalysts investigated here agrees well with that reported in an earlier study [14].
2. Under the reaction conditions of the present study, the unconditioned catalysts deactivated strongly, much more pronounced than the conditioned catalysts prepared in the same way (except for conditioning), in contrast to previous findings [14]. Apparently, any reaction-induced activation of the catalyst, compensating for the simultaneous deactivation, was a minor effect compared with the deactivation.
3. Based on the TEM results, which indicate that the average Au particle size grew only from 1.3 to 1.8 nm, Au particle growth can be ruled out as main origin for the deactivation.

4. XPS and DRIFTS data in combination show that after drying in air (50 °C), the catalyst consisted of very small, possibly slightly charged $Au^0$ particles and fully oxidized $Ti^{4+}$, with negligible contributions of cationic $Au^{\delta+}$ and $TiO^{3+}$ species, and the chemical composition of the catalyst surface changed very little during the reaction.
5. The deactivation of the unconditioned catalysts was correlated with the build-up of surface carbonates.
6. The $CO_{ad}$ coverage (CO adsorbed on the Au nanoparticles), $CO_2$ formation rate, and surface carbonate coverage were closely correlated, as evidenced by the DRIFTS data.
7. At 80 °C, surface carbonate formation was reduced in the presence of $O_2$, which we tentatively attribute to an oxygen-induced enhanced carbonate decomposition. This resulted in a slower increase and lower steady-state carbonate coverage in a $O_2$-rich reaction atmosphere under these conditions compared with those in the standard reaction atmosphere.

Considering that Au particle growth during the CO oxidation was negligible for both the unconditioned catalyst and the similarly prepared calcined catalyst [24], the much stronger deactivation of the unconditioned Au/TiO$_2$ catalyst compared with calcined Au/TiO$_2$ catalysts must be due to a more pronounced effect from surface carbonate formation. Because the present data do not allow a quantitative comparison of the carbonate coverage (i.e., of the fraction of the titania support covered by carbonates), the enhanced deactivation of the unconditioned catalysts may reflect either increased carbonate formation or an enhanced effect of surface carbonates on CO adsorption and $CO_2$ formation. Experiments are planned to investigate this question in more detail.

The correlation between carbonate coverage on the one hand and $CO_{ad}$ intensity/$CO_2$ formation rate on the other hand can be explained most simply through a mechanistic picture in which the $CO_{ad}$ coverage is rate-limiting and CO adsorption sites are increasingly blocked by adsorbed carbonates. In the literature, however, the C–O stretch signal at 2112 cm$^{-1}$ is generally attributed to CO adsorbed on metallic Au nanoparticles [13,17], whereas the surface carbonates associated with the characteristic IR signals at 1527 and 1357 cm$^{-1}$ are adsorbed on the TiO$_2$ support [39]. Therefore, they should not affect the $CO_{ad}$ coverage on the Au nanoparticles. Resolving this discrepancy would require either carbonate adsorption on the Au nanoparticles (which contradicts the commonly accepted assignment of the IR data) or the presence of a minority species of surface carbonates adsorbed on Au. Whereas earlier attempts to produce surface carbonates on Au surfaces were unsuccessful [47], in contrast to the facile formation of surface carbonates on Ag(110) [48–50], we cannot rule out carbonate formation also on the Au nanoparticles. The vibrational feature at 1343 cm$^{-1}$ observed for carbonates on Ag(110), which was attributed to the asymmetric O–C–O vibration ($\nu_{as}$(OCO)) of planar carbonate on Ag(110), would be buried in the broad vibrational band of the majority carbonate species adsorbed on the oxide. Another way to explain the present results is based on a reaction scheme in which the $CO_{ad}$ supply occurs not only by

direct CO adsorption on the Au particles, but also (or even predominately) by adsorption on the $TiO_2$ support and subsequent reverse spillover on the Au nanoparticles. In that reaction scheme, the increasing carbonate coverage on the support reduces the supply of $CO_{ad}$ to the Au nanoparticles and thus also the steady-state $CO_{ad}$ coverage on the Au particles and, consequently, also the supply of $CO_{ad}$ to the active sites for reaction. As a result, both $CO_{ad}$ intensity and CO oxidation activity should decay, in agreement with the experimental observations. This explanation is supported by the observed shift of the C–O vibration to higher frequencies with reaction time, pointing to a decreased local density of the CO adlayer on the Au nanoparticles with time [42]. This reaction mechanism closely resembles our recent proposal for the water–gas shift reaction on $Au/CeO_2$ catalysts, where we arrived at a similar conclusion based on the correlation among the Au surface-normalized activity, the coverage of bidentate formats, and that of reaction-inhibiting monodentate carbonates [51].

The tentative proposal of an oxygen-induced enhanced decomposition of the surface carbonate compared with an oxygen-related inhibition of carbonate formation is supported by recent data from a temporal analysis of products reactor showing $CO_2$ formation when pulsing $O_2$ on a carbonate-covered $Au/TiO_2$ catalyst [52].

The formation of small amounts of bicarbonates, by reaction of carbonates with $H_2O$ and OH groups present on the surface at the beginning of the reaction, may affect the effective measured carbonate formation rate by continuous removal of carbonates through bicarbonate formation and subsequent decomposition. The steady-state coverage of these bicarbonates must be constant, as evidenced by the constant intensity of the OH- and $H_2O$-related signals. However, for the reaction mechanism, it is important to note that this continuous loss of carbonate is small compared with carbonate formation. Therefore, the buildup of carbonates on the catalyst remains the decisive factor in the deactivation of the catalyst; see also [53–56] for information on the role of $H_2O$ in reactivity.

Finally, we mention that the pronounced tendency for carbonate formation identified as the main reason for the rapid deactivation of these $Au/TiO_2$ catalysts at low temperatures is, at least so far, limited to catalysts based on the same $TiO_2$ support material used in this study (P25). Strategies for future work should concentrate on optimizing the support material toward reduced activity for carbonate formation or, equivalently, enhanced activity for carbonate decomposition. For applications in fuel gas processing, where CO must be removed from $H_2$-rich feed gases, carbonate formation is less limiting because of the reduced stability of carbonates in a $H_2O$-containing atmosphere, most likely due to preferred formation of less stable bicarbonates under these conditions (see [8]).

## 5. Conclusion

Combining kinetic and in situ IR spectroscopic measurements of the reaction and deactivation process, as well as ex situ catalyst characterization before an after the reaction, we could demonstrate that unconditioned $Au/TiO_2$ catalysts based on

commercial support material (P25) deactivated very strongly during CO oxidation at both 30 and at 80 °C and in standard reaction mixtures and in an $O_2$-rich atmosphere. Both before and after reaction, the catalyst consisted of fully oxidized support material ($Ti^{4+}$) and very small, possibly slightly charged $Au^0$ particles, with only negligible contributions from $Ti^{3+}$ and cationic $Au^{\delta+}$ species. The deactivation, which was much more pronounced than that for calcined Au catalyst prepared from the same support material, was correlated with and assigned to the buildup of surface carbonates on the support. Reaction-induced growth of the very small Au particles was slight, from $1.3 \pm 0.4$ nm before to typically $1.8 \pm 0.8$ nm after a 2000-min reaction, and can be excluded as dominant reason for the deactivation. The close correlation between carbonate buildup and decay in $CO_{ad}$ coverage (on the Au particles) as well as $CO_2$ formation can be tentatively explained by a model in which the $CO_{ad}$ supply on the Au nanoparticles occurs to a large extent through adsorption on the support and subsequent reverse spillover on the Au particles. Accordingly, increased blocking of the support resulted in a corresponding decay of the $CO_{ad}$ steady-state coverage and of the $CO_{ad}$ supply for $CO_2$ formation, that is, in a similar decay of the $CO_2$ formation rate.

## Supplementary material

The online version of this article contains additional supplementary material.

Please visit DOI: 10.1016/j.jcat.2007.07.029.

## References

[1] G.C. Bond, D.T. Thompson, Catal. Rev. Sci. Eng. 41 (1999) 319.
[2] G. Mul, A. Zwijnenburg, B. van der Linden, M. Makkee, J.A. Moulijn, J. Catal. 201 (2001) 128.
[3] M. Haruta, Gold Bull. 37 (2004) 27.
[4] M. Haruta, Catal. Surv. Jpn. 1 (1997) 61.
[5] F. Boccuzzi, A. Chiorino, J. Phys. Chem. B 104 (2000) 5414.
[6] G.C. Bond, D.T. Thompson, Gold Bull. 33 (2000) 41.
[7] M. Haruta, CATECH 6 (2002) 102.
[8] B. Schumacher, Y. Denkwitz, V. Plzak, M. Kinne, R.J. Behm, J. Catal. 224 (2004) 449.
[9] B. Schumacher, V. Plzak, J. Cai, R.J. Behm, Catal. Lett. 101 (2004) 215.
[10] R. Zanella, S. Giorgio, C.-H. Shin, C.R. Henry, C. Louis, J. Catal. 222 (2004) 357.
[11] P. Konova, A. Naydenov, Cv. Venkov, D. Mehandjiev, D. Andreeva, T. Tabakova, J. Mol. Catal. A 213 (2004) 235.
[12] Q. Fu, H. Saltsburg, M. Flytzani-Stephanopoulos, Science 301 (2003) 935.
[13] M. Haruta, S. Tsubota, T. Kobayashi, H. Kageyama, M.J. Genet, B. Delmon, J. Catal. 144 (1993) 175.
[14] E.A. Willneff, S. Braun, D. Rosenthal, H. Bluhm, M. Hävecker, E. Kleimenov, A. Knop-Gericke, R. Schlögl, S.L.M. Schroeder, J. Am. Chem. Soc. 128 (2006) 12052.
[15] Y. Iizuka, H. Fujiki, N. Yamauchi, T. Chijiiwa, S. Arai, S. Tsubota, M. Haruta, Catal. Today 36 (1997) 115.

[16] A.I. Kozlov, A.P. Kozlova, H. Liu, Y. Iwasawa, Appl. Catal. A 182 (1999) 9.
[17] J.-D. Grunwaldt, A. Baiker, J. Phys. Chem. B 103 (1999) 1002.
[18] F. Boccuzzi, A. Chiorini, M. Manzoli, P. Lu, T. Akita, S. Ichikawa, M. Haruta, J. Catal. 202 (2001) 256.
[19] J. Guzman, B.C. Gates, J. Am. Chem. Soc. 126 (2004) 2672.
[20] S.T. Daniells, A.R. Overweg, M. Makkee, J.A. Moulijn, J. Catal. 230 (2005) 52.
[21] L. Fu, N.Q. Wu, J.H. Yang, F. Qu, D.L. Johnson, M.C. Kung, H.H. Kung, V.P. Dravid, J. Phys. Chem. B 109 (2005) 3704.
[22] G.J. Hutchings, M.S. Hall, A.F. Carley, P. Landon, B.E. Solsona, C.J. Kiely, A. Herzing, M. Makkee, J.A. Moulijn, A. Overweg, J.C. Fierro-Gonzalez, J. Guzman, B.C. Gates, J. Catal. 242 (2006) 71.
[23] M.P. Casaletto, A. Longo, A. Martorana, A. Prestianni, A.M. Venezia, Surf. Interface Anal. 38 (2006) 215.
[24] B. Schumacher, V. Plzak, M. Kinne, R.J. Behm, Catal. Lett. 89 (2003) 109.
[25] M. Valden, X. Lai, D.W. Goodman, Science 281 (1998) 1647.
[26] B. Schumacher, Ph.D. thesis, Ulm University, 2005.
[27] V. Plzak, J. Garche, R.J. Behm, Eur. Fuel Cell News 10 (2003) 16.
[28] J.F. Moulder, W.F. Stickle, P.E. Sobol, K.D. Bomben, Handbook of X-Ray Photoelectron Spectroscopy, Perkin–Elmer Corporation, Eden Prairie, 1992.
[29] M.J. Kahlich, H.A. Gasteiger, R.J. Behm, J. Catal. 171 (1997) 93.
[30] P.B. Weisz, Chem. Eng. Prog. Symp. Ser. 55 (1992) 29.
[31] M.M. Schubert, M.J. Kahlich, H.A. Gasteiger, R.J. Behm, J. Power Sources 84 (1999) 175.
[32] I.M. Hamadeh, P.R. Griffiths, Appl. Spectrosc. 41 (1987) 682.
[33] J. Sirita, S. Phanichphant, F.C. Meunier, Anal. Chem. 79 (2007) 3912.
[34] S. Kielbassa, M. Kinne, R.J. Behm, J. Phys. Chem. B 108 (2004) 19184.
[35] B. Schumacher, Y. Denkwitz, V. Plzak, R.J. Behm, in preparation.
[36] R. Holm, S. Storp, Appl. Phys. 9 (1976) 217.
[37] G.K. Wertheim, S.B. DiCenzo, S.E. Youngquist, Phys. Rev. Lett. 51 (1983) 2310.
[38] H.-G. Boyen, A. Ethirajan, G. Kästle, F. Weigl, P. Ziemann, G. Schmid, M.G. Garnier, M. Büttner, P. Oelhafen, Phys. Rev. Lett. 94 (2005) 016804.
[39] A.A. Davydov, Infrared Spectroscopy of Adsorbed Species on the Surface of Transition Metal Oxides, Wiley, Chichester, 1984.
[40] M.A. Bollinger, M.A. Vannice, Appl. Catal. B 8 (1996) 417.
[41] J.-D. Grunwaldt, M. Maciejewski, O.S. Becker, P. Fabrizioli, A. Baiker, J. Catal. 186 (1999) 458.
[42] J. France, P. Hollins, J. Electron Spectrosc. Relat. Phenom. 64–65 (1993) 251.
[43] K.S. Kim, M.A. Barteau, Langmuir 4 (1988) 945.
[44] K.S. Finnie, D.J. Cassidy, J.R. Bartlett, J.L. Woolfrey, Langmuir 17 (2001) 816.
[45] M.I. Zaki, H. Knözinger, Mater. Chem. Phys. 17 (2003) 201.
[46] P. Jackson, G.D. Parfitt, J. Chem. Soc. Faraday Trans. 68 (1972) 897.
[47] D.A. Outka, R.J. Madix, Surf. Sci. 179 (1987) 351.
[48] M.A. Barteau, R.J. Madix, J. Electron Spectrosc. Relat. Phenom. 31 (1983) 101.
[49] E.M. Stuve, R.J. Madix, B.A. Sexton, Chem. Phys. Lett. 89 (1982) 48.
[50] L. Constant, B. Krenzer, W. Stenzel, H. Conrad, A.M. Bradshaw, Surf. Sci. 427–428 (1999) 262.
[51] R. Leppelt, B. Schumacher, V. Plzak, M. Kinne, R.J. Behm, J. Catal. 244 (2006) 137.
[52] M. Kotobuki, D. Widmann, R. Leppelt, R.J. Behm, in preparation.
[53] M. Daté, M. Haruta, J. Catal. 201 (2001) 221.
[54] M. Daté, M. Okumura, S. Tsubota, M. Haruta, Angew. Chem. 116 (2004) 2181.
[55] M.A. Debeila, R.P.K. Wells, J.A. Anderson, J. Catal. 239 (2006) 162.
[56] M. Azar, V. Caps, F. Morfin, J.-L. Rousset, A. Piednoir, J.-C. Bertolini, L. Piccolo, J. Catal. 239 (2006) 307.